Motion of holes on the triangular lattice studied using the *t-J* model

Mohamed Azzouz
Centre de Recherche en Physique du Solide et Département de Physique, Université de Sherbrooke, Québec, Canada J1K 2R1

Thierry Dombre
CNRS, Centre de Recherche sur les Tres Basses Températures, Boîte Postale 166, 38042 Grenoble, Cédex 9, France
(Received 23 February 1995)

The motion of holes on the triangular lattice is studied using the *t-J* model. Within the Born self-consistent approximation and the exact Lanczos diagonalization, the single-hole physics is first analyzed. Then the spiral phase theory of Shraiman and Siggia is used to investigate the case of a finite density of holes.

I. INTRODUCTION

The main motivation for the recent innumerable works on the Hubbard model is the Anderson suggestion[1] that says that this model, in its simple version, can explain the physics of the CuO planes in high critical temperature superconductors. The Hamiltonian of this model is written as follows:

$$H=-t\sum_{\langle i,j\rangle}(c^{\dagger}_{i,\sigma}c_{j,\sigma}+\text{H.c})+U\sum_{i}n_{i,\uparrow}n_{i,\downarrow} \tag{1}$$

where $n_{i,\sigma}=c^{\dagger}_{i,\sigma}c_{i,\sigma}$ is the occupation number of an electron with a spin σ at the site i. The first term of H is the kinetic energy which allows for an electron to hop from one site to one of its nearest neighbors with an amplitude t. The second term stands for the on-site Coulomb repulsion ($U>0$) and $c^{\dagger}_{i,\sigma}$ and $c_{i,\sigma}$ are respectively creation and annihilation operators.

For large U, the double occupancy of a site with two electrons $\uparrow$ and $\downarrow$ is energetically discarded. In this limit the Hubbard model becomes equivalent to the so-called *t-J* model:

$$H_{t\text{-}J}=P_0\left\{-t\sum_{\langle i,j\rangle}(c^{\dagger}_{i,\sigma}c_{j,\sigma}+\text{H.c.})\right\}P_0 + J\sum_{\langle i,j\rangle}\left(\mathbf{S}_i\cdot\mathbf{S}_j-\frac{1}{4}n_in_j\right) \tag{2}$$

where $P_0=\Pi_i(1-n_{i,\uparrow}n_{i,\downarrow})$ applies the constraint of non double occupancy. $\mathbf{S}=(1/2)\Sigma_{\alpha,\beta}c^{\dagger}_{i,\alpha}\boldsymbol{\sigma}_{\alpha,\beta}c_{i,\beta}$ is the spin operator (σ^x, σ^y, and σ^z are the Pauli matrices). The coupling constant of the magnetic part, $J=4t^2/U$, is positive.

At half filling (one electron per site on average), the first term of H_{t-J} is effectiveless and the model reduces to the Heisenberg model. It is now widely believed that the ground state ($T=0$ K) of the Heisenberg model on the square and triangular lattices presents antiferromagnetic long range order in the thermodynamic limit.[2]

In this paper, the motion of a single hole is first studied on the triangular lattice using the slave fermion representation and an exact diagonalization. Then the collective instabilities for a finite density of holes are investigated in the framework of a mean-field approach introduced by Shraiman and Siggia[3] and known to lead to spiral phases. The main result in that part of our work is that spiral phases in the doped case can only develop within the preexisting plane of the 120° antiferromagnetic (AF) structure of the pure system. The discussion of the present results is made together with a comparison with the square lattice results.

In the second section, the slave fermion representation is used to write down an effective Hamiltonian from (2). Section III describes the self-consistent Born approximation within which the single-particle properties are calculated. The results, analyzed in Secs. IV and V, distinguish between the cases $J\neq 0$ and $J=0$. For the former case a *Fermi liquid* description can be done. However, for the latter one and for positive t, the quasiparticle vanishes away from the center of the Brillouin zone. The question of a ''liquid'' where the quasiparticle depends on the position of the wave vector on the Brillouin zone arises naturally and will be addressed elsewhere. Section VI is devoted to an exact calculation using the Lanczos method. Good agreement concerning the position of the energy minima as a function of $\mathbf{k}$ is obtained. Finaly, the motion of a finite density of holes is considered in Secs. VII and VIII where the spiral phase is calculated.

II. THE MODEL

A. Slave fermion representation

The *t-J* model is characterized by the existence of spin and charge degrees of freedom. In one dimension (1D), these degrees of freedom separate and one ends with a free propagation of the hole and the domain wall in the AF background. This illustrates the mechanism of spin-charge separation in 1D. In 2D, a string of unsatisfied bonds occurs behind the moving hole. Spin and charge degrees *remain coupled.*

The constrained electronic operator is written as follows:

$$c_{i,\sigma}(1-n_{i,\sigma})\equiv\tilde{c}_{i,\sigma}=\psi^{\dagger}_i b_{i,\sigma} \tag{3}$$

where $\psi^{\dagger}_i$ is a fermionic operator which creates a spinless hole at the site i and $b^{\dagger}_{i,\sigma}$ is the Schwinger boson[4] operator which creates a spin σ at i. The number of bosons and fermions on each site must satisfy the following constraint:

$$\psi^{\dagger}_i\psi_i+\sum_{\sigma}b^{\dagger}_{i,\sigma}b_{i,\sigma}=2S. \tag{4}$$

The spin operator is written in the form

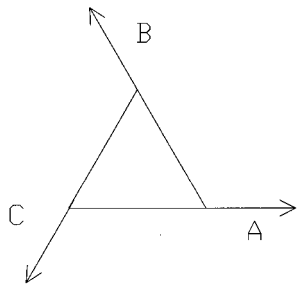

FIG. 1. The *classical Néel state* in the case of the triangular lattice is drawn on one plaquette. The three sublattices A, B, and C are shown as well. $\mathbf{e}_i$ correspond respectively to the vectors on A, B, and C sublattices for $i=1$, $i=2$, and $i=3$.

$$\vec{\mathbf{S}}_i=\chi_i^\dagger\vec{\boldsymbol{\sigma}}\chi_i, \tag{5}$$

where

$$\chi_i=\begin{pmatrix} b_{i,\uparrow} \\ b_{i,\downarrow}\end{pmatrix} \tag{6}$$

is a two-component spinor. The Schwinger boson formalism is easily generalized to higher values of the spin S where an expansion on $1/2S$ allows one to recover the spin wave theory, that is,

$$\chi_i=\begin{pmatrix} \sqrt{2S-b_i^\dagger b_i} \\ b_i\end{pmatrix}\approx\begin{pmatrix} \sqrt{2S}-b_i^\dagger b_i/2\sqrt{2S} \\ b_i\end{pmatrix} \tag{7}$$

for large S. Here b_i is the Holstein-Primakoff bosonic operator describing small deviations around the classical spin configuration which minimizes the energy (this configuration is hereafter called the classical Néel state as on the square lattice):

$$\chi_i=\begin{pmatrix} 2S \\ 0\end{pmatrix}. \tag{8}$$

The constraint (4) is transformed into a nonholonomic constraint

$$\psi_i^\dagger\psi_i+b_i^\dagger b_i\leqslant 2S \tag{9}$$

which is more difficult to handle than (4). The latter is taken into account by introducing a site-dependent Lagrange multiplier λ_i and the effective action is written as follows:

$$\begin{aligned}\mathcal{S}=\int_0^\beta \mathrm{d}\tau\Bigg\{ &-t\sum_i\ \psi_i^\dagger\partial_\tau\psi_i+\sum_i\ b_{i,\sigma}^\dagger\partial_\tau b_{i,\sigma} \\ &-t\sum_{\langle i,j\rangle}\ \psi_i^\dagger\psi_j b_{j,\sigma}b_{i,\sigma}^\dagger+J\sum_{\langle i,j\rangle}\left(\frac{1}{2}\chi_i^\dagger\boldsymbol{\sigma}\chi_i\right)\left(\frac{1}{2}\chi_j^\dagger\boldsymbol{\sigma}\chi_j\right) \\ &+\sum_i\ \lambda_i(\psi_i^\dagger\psi_i+\chi_i^\dagger\chi_i-2S)\Bigg\}.\end{aligned} \tag{10}$$

In the spin wave theory the constraint is neglected and we do so in the present work.

B. Effective Hamiltonian on the triangular lattice

The classical Néel state on the triangular lattice is displayed in Fig. 1. The spins are oriented, on a coplanar configuration, in such a way that two adjacent spins make an angle of $2\pi/3$. These different orientations define three sublattices A, B, and C instead of two sublattices as is the case on the square lattice where two adjacent spins are antiparallel. By carrying out a local rotation of $2\pi/3$ and $-2\pi/3$ on the sublattices B and C, respectively, that is,

$$\chi_{B(C)}=\mathscr{R}_{B(C)}\begin{pmatrix} \sqrt{1-b^\dagger b} \\ ib\end{pmatrix} \tag{11}$$

where $\mathscr{R}_{B(C)}$ is the SU(2) matrix representing the rotation on $B(C)$, the system is made formally ferromagnetic but the resulting Hamiltonian keeps naturally its AF character:

$$\begin{aligned}H_{t\text{-}J}\rightarrow H=&-\frac{t}{2}\sum_{\langle i,j\rangle}\ (\psi_i^\dagger\psi_j+\mathrm{H.c.})-\frac{t}{2}\sum_{\langle i,j\rangle}\ (\psi_j^\dagger\psi_j b_j^\dagger b_i+\mathrm{H.c.})-\frac{t\sqrt{3}}{2}\left(\sum{}'\ \psi_i^\dagger\psi_j(b_i-b_j^\dagger)-\sum{}''\psi_i^\dagger\psi_j(b_i-b_j^\dagger)\right) \\ &+\frac{3J}{2}\sum_i\ b_i^\dagger b_i+\frac{J}{8}\sum_{\langle i,j\rangle}\ [b_i^\dagger b_j+b_j^\dagger b_i-3(b_i b_j+b_j^\dagger b_i^\dagger)].\end{aligned} \tag{12}$$

The hole moves as a free particle (coherent motion) through the first term in (12) which is present since the spinors on adjacent sites are not orthogonal. In the case of the square lattice, such a term is absent. The second term in (12) allows an exchange of a spin flip and the hole by conserving the total number of overturned spins. In the third term, there is a change in the sign depending on whether the spin flip is absorbed or created after the hopping of the hole. Σ' (Σ'') refers to the propagation of the hole in the three directions $\mathbf{e}_i$ ($-\mathbf{e}_i$), Fig. 1. The last term is the AF exchange interaction written in spin wave theory.

The presence of coherent and incoherent propagations of the hole is a salient feature of the triangular antiferromagnetic lattice, which in some sense interpolates between the ferromagnetic and antiferromagnetic limits on the square lattice. In the last case, only incoherent propagation is possible in the absence of quantum spin fluctuations. Arguments taken from the Brinkman-Rice picture[5] show that the most important hopping terms in (12) are the first and the third. The point is that the coherent propagation alone would give a minimum in the hole dispersion of $-3t$ for $t>0$ or of $3t/2$ for $t<0$. But the hole can still lower its kinetic energy in a quite significant manner by using the incoherent channel. Indeed, were the third term alone, then the estimate $-t\sqrt{15}$ obtained in the self-retracing path approximation would ap-

ply. On the other hand, we expect the second term to play only a minor role and shall therefore neglect it in the following.

Transcribed in **k** space, Eq. (12) yields

$$H=-it\frac{\sqrt{3}}{N}\sum_{\mathbf{k},\mathbf{q}}\psi^{\dagger}_{\mathbf{k}+\mathbf{q}}\psi_{\mathbf{k}}[(u_{\mathbf{q}}h_{\mathbf{k}}-v_{\mathbf{q}}h_{\mathbf{k}+\mathbf{q}})\alpha_{\mathbf{q}}+(v_{\mathbf{q}}h_{\mathbf{k}}-u_{\mathbf{q}}h_{\mathbf{k}+\mathbf{q}})\alpha^{\dagger}_{-\mathbf{q}}]-t\sum_{\mathbf{k}}\gamma_{\mathbf{k}}\psi^{\dagger}_{\mathbf{k}}\psi_{\mathbf{k}}+J\sum_{\mathbf{q}}\omega_{\mathbf{q}}\alpha^{\dagger}_{\mathbf{q}}\alpha_{\mathbf{q}} \quad (13)$$

where

$$\gamma_{\mathbf{k}}=\sum_{\mathbf{e}_i}\cos(\mathbf{k}\cdot\mathbf{e}_i), \quad h_{\mathbf{k}}=\sum_{\mathbf{e}_i}\sin(\mathbf{k}\cdot\mathbf{e}_i),$$

and

$$\omega_{\mathbf{q}}=\frac{3}{2}J\sqrt{\left(1-\frac{\gamma_{\mathbf{q}}}{3}\right)\left(1+\frac{2\gamma_{\mathbf{q}}}{3}\right)}.$$

The operator $\alpha_{\mathbf{q}}$ obtained from $b_{\mathbf{q}}$ by using the Bogoliubov transformation creates a spin wave with a wave vector **q**. $u_{\mathbf{q}}$ and $v_{\mathbf{q}}$ are the coherence factors:

$$u_{\mathbf{q}}=\sqrt{\frac{J}{2\omega_{\mathbf{q}}}}\sqrt{\frac{3}{2}+\frac{\gamma_{\mathbf{q}}}{4}+\frac{\omega_{\mathbf{q}}}{J}},$$

$$v_{\mathbf{q}}=\mathrm{sgn}(-\gamma_{\mathbf{q}})\sqrt{\frac{J}{2\omega_{\mathbf{q}}}}\sqrt{\frac{3}{2}+\frac{\gamma_{\mathbf{q}}}{4}-\frac{\omega_{\mathbf{q}}}{J}}.$$

In the following, (13) is investigated using the self-consistent Born approximation as developed in Ref. 6.

III. SELF-CONSISTENT BORN APPROXIMATION

The single-particle Green's function is defined as follows:

$$G_{\sigma}(\mathbf{k},\omega)=\left\langle \Phi_0\left|c^{\dagger}_{\mathbf{k},\sigma}\frac{1}{\omega-H}c_{\mathbf{k},\sigma}\right|\Phi_0\right\rangle \quad (14)$$

where $|\Phi_0\rangle$ is the ground state of the AF Heisenberg part of the Hamiltonian. Using (3) one gets

$$c_{k,\sigma}=\frac{1}{\sqrt{N}}\sum_{k'}\psi^{\dagger}_{k'}b_{k+k',\sigma} \quad (15)$$

for the electronic operator in the slave fermion representation. As an approximation, the operator $b_{k+k',\sigma}$ is replaced by its mean value in the Néel configuration since we consider that the important physics is contained in the fermionic part ψ. We define the Green's function related to ψ by

$$G(\mathbf{k},\omega)=\left\langle \Phi_0\left|\psi_k\frac{1}{\omega-H}\psi^{\dagger}_k\right|\Phi_0\right\rangle. \quad (16)$$

In the Néel state, we have

$$\langle b_{i,\uparrow}\rangle\approx\exp(2im\pi/3) \text{ and } \langle b_{i,\downarrow}\rangle\approx\exp(-2im\pi/3)$$

where m takes the values 0, 1, and -1 on the three sublattices A, B, and C, respectively. This can be written in the form

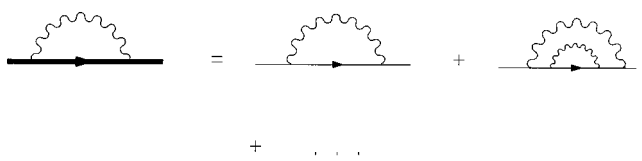

FIG. 2. On the left hand side of the figure, the diagram used for self-energy is shown (with the bare propagator substituted by the true one). The expansion in the bare propagator is shown on the right hand side. The wavy line refers to the spin wave propagator.

$$\langle b_{i,\uparrow}\rangle\approx\exp(-i\mathbf{G}\cdot\mathbf{R}_i) \text{ and } \langle b_{i,\downarrow}\rangle\approx\exp(i\mathbf{G}\cdot\mathbf{R}_i)$$

where $\mathbf{G}=(4\pi/3)x$. Transcribed in Fourier space, these yield

$$\langle b_{k,\uparrow}\rangle\approx\sqrt{N}\delta_{\mathbf{k},-\mathbf{G}} \text{ and } \langle b_{k,\downarrow}\rangle\approx\sqrt{N}\delta_{\mathbf{k},\mathbf{G}}.$$

A simple correspondence between the true Green's function, (14), and the ψ Green's function, (16), namely,

$$G_{\uparrow}(\mathbf{k},\omega)\approx G(-\mathbf{k}-\mathbf{G},\omega), \quad G_{\downarrow}(\mathbf{k},\omega)\approx G(-\mathbf{k}+\mathbf{G},\omega), \quad (17)$$

allows the evaluation of the true electronic Green's function G_{σ} using G. In this section, we concentrate on the Green's function of the slave fermion.

The Dyson equation for $G(\mathbf{k},\omega)$ is

$$G(\mathbf{k},\omega)=\frac{1}{\omega-\epsilon(\mathbf{k})-\Sigma(\mathbf{k},\omega)} \quad (18)$$

where $\epsilon(\mathbf{k})=-t\gamma(\mathbf{k})$ is the free part of the kinetic energy and $\Sigma(\mathbf{k},\omega)$ is the self-energy resulting from the incoherent motion of the hole. The evaluation of $\Sigma(\mathbf{k},\omega)$ is done using the diagram of Fig. 2 which corresponds to the following expression:

$$\Sigma(\mathbf{k},\omega)=\frac{3t^2}{N}\sum_{\mathbf{q}}|M(\mathbf{k},\mathbf{q})|^2G^{(0)}(\mathbf{k}+\mathbf{q},\omega-\omega(\mathbf{q})) \quad (19)$$

where $G^{(0)}$ is the ψ Green's function of the free part of the Hamiltonian. The self-consistent approximation consists in replacing $G^{(0)}$ in (19) by the total Green's function G. In this approximation, (18) becomes

$$G(\mathbf{k},\omega)=\left(\omega-\epsilon(\mathbf{k})-\frac{3t^2}{N}\sum_{\mathbf{q}}|M(\mathbf{k},\mathbf{q})|^2G(\mathbf{k}+\mathbf{q},\omega-\omega(\mathbf{q}))\right)^{-1} \quad (20)$$

where $M(\mathbf{k},\mathbf{q})=v_qh_k-u_qh_{k+q}$.

In this approach, a series of an infinite number of diagrams which neglect vertex corrections is considered as shown in Fig. 2. Vertex corrections roughly correspond to Trugman processes,[7] which are known to become important for $t\gg J$. In the most elementary process of this type on the triangular lattice, the hole makes one turn and a half around a triangular plaquette, which gives rise to coherent nearest-neighbor hopping. Trugman processes tend to push the energy minima towards the corners of the hexagonal Brillouin

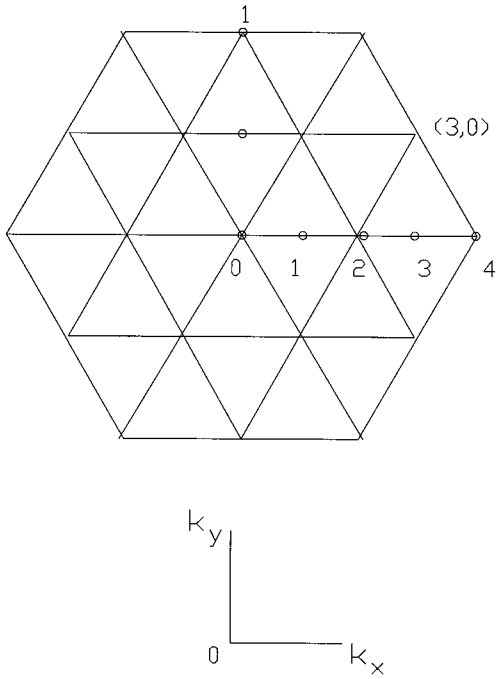

FIG. 3. The Brillouin zone is displayed for $\ell=2$. In this case, the wave vectors $\mathbf{k}=(0,0)$, $(\pi,\pi/3^{1/2})$, and $(4\pi/3,0)$ correspond, respectively, to the points $(m,n)=(0,0)$, $(3,0)$, and $(4,0)$.

zone (independent of the sign of t). Their influence should remain weak for moderate values of J/t, as on the square lattice.

IV. RESULTS

Equation (20) is computed by means of an iterative method. We fix an arbitrary initial function $G(\mathbf{k},\omega)$ for all wave vectors $\mathbf{k}$, belonging to the hexagonal Brillouin zone, and frequencies ω, and use (20) to iterate until convergence towards the unique solution. The uniqueness has been proved by starting from different initial functions.

The numerical calculation is performed for hexagonal clusters where the sites are labeled as shown in Fig. 3 and parametrized as follows

$$k_x=\frac{2\pi}{3\ell}m, \quad 0\leq m<3\ell,$$

$$k_y=\frac{4\pi}{\sqrt{3}\ell}\left(n+\frac{1}{2}\frac{1-(-1)^m}{2}\right), \quad 0\leq n<\ell, \tag{21}$$

to get the right number of independent sites inside the first Brillouin zone. The results presented here are from a cluster of 108 sites ($\ell=6$). The number of independent sites is $3\ell^2$.

The quantity of interest is the spectral function which is related to the Green's function through the relation

$$\mathcal{A}(\mathbf{k},\omega)=-\frac{1}{\pi}\,\mathrm{Im}G(\mathbf{k},\omega). \tag{22}$$

At finite J, $\mathcal{A}(\mathbf{k},\omega)$ presents a $\mathbf{k}$-dependent quasiparticle peak at low energies. This is consistent with a Fermi liquid picture for positive and negative t. Note that, because the electron-hole symmetry is absent for the t-J model on the triangular lattice, the spectral function depends on the sign of t. This is not the case on the square lattice where there is a $t\rightarrow -t$ symmetry.

For negative t and finite J, the energy minimum of the quasiparticle peak is located at $\mathbf{k}=(\pi,\pi/\sqrt{3})$ which corresponds to the middle of the edges of the Brillouin zone. For positive t, however, the minimum is realized at the center of the Brillouin zone: $\mathbf{k}=(0,0)$. The spectral functions of these wave vectors, together with those of $\mathbf{k}=(4\pi/3,0)$, are displayed in Fig. 4 and Fig. 5 for $J/|t|=0.2$.

V. PROPERTIES OF THE QUASIPARTICLE

A. Spectral weight of the quasiparticle for $t<0$

In this section, we are interested in analyzing the properties of the quasiparticle in the case of negative t. The spectral weight $a(\mathbf{k})$ of the quasiparticle is calculated by computing the area under the quasiparticle peak. The results for small values of J suggest a simple power law as a function of J:

$$a(\mathbf{k})\simeq\beta J^{\alpha} \tag{23}$$

where the values of α and β are summarized in Table I for the three characteristic wave vectors $\mathbf{k}=(0,0)$, $(4\pi/3,0)$, and $(\pi,\pi/\sqrt{3})$. $a(\mathbf{k})$ is $\mathbf{k}$ dependent. The zero quasiparticle weight at $J=0$ implies the absence of the quasiparticle peak at low energies as may be shown by the spectral function. What the absence of the quasiparticle means is the breakdown of the Fermi liquid picture. However, the Nagaoka theorem[8] applies for negative t and ensures that the ground state is ferromagnetic at $U=\infty$ ($J=4t^2/U$). Our result in this case is an artifact of the approximation which states an AF background. For finite J, it is natural to consider such a background and our results are physically meaningful.

For $J\gg|t|$, the spectral weight goes to unity since

$$a(\mathbf{k})=\frac{1}{1-(\partial/\partial\omega)\mathrm{Re}\Sigma(\mathbf{k},\omega)}, \quad \omega=E(\mathbf{k}),$$

and

$$\frac{\partial}{\partial\omega}\mathrm{Re}\Sigma(\mathbf{k},\omega)\simeq-\frac{3t^2}{N}\sum_{\mathbf{q}}\frac{|M(\mathbf{k},\mathbf{q})|^2}{[\omega(\mathbf{q})-t\gamma_{\mathbf{k}}]^2}\sim\frac{t^2}{J^2}.$$

B. Quasiparticle dispersion relation for $t<0$

By performing the numerical calculation of the position of the quasiparticle peak for every wave vector belonging to the Brillouin zone, we get the dispersion in $\mathbf{k}$ of the energy minimum. This energy is well fitted by the following simple expression

$$E(\mathbf{k})=A+B\gamma_{\mathbf{k}}+Ch_{\mathbf{k}}^2 \tag{24}$$

suggested by the arguments developed in Ref. 9. A, B, and C are J dependent as seen in Table II.

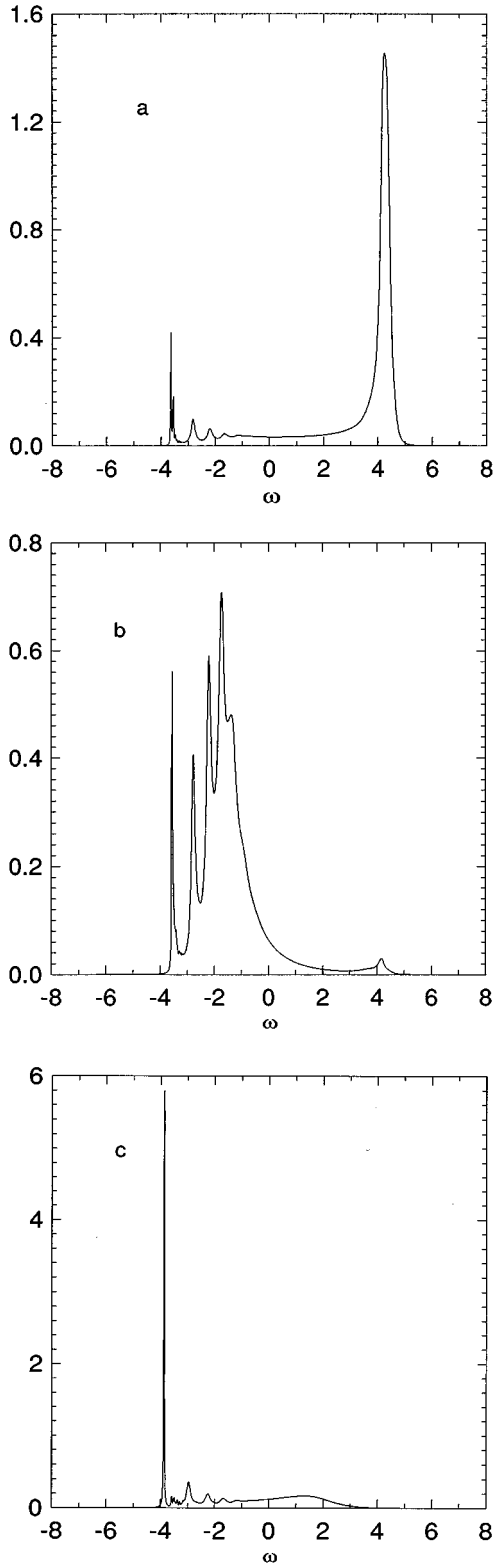

FIG. 4. The spectral functions of (a) (0,0), (b) $(4\pi/3,0)$, and (c) $(\pi,\pi/3^{1/2})$ are presented as a function of frequency. $\ell=6$, $t=-1$, and $J=0.2|t|$.

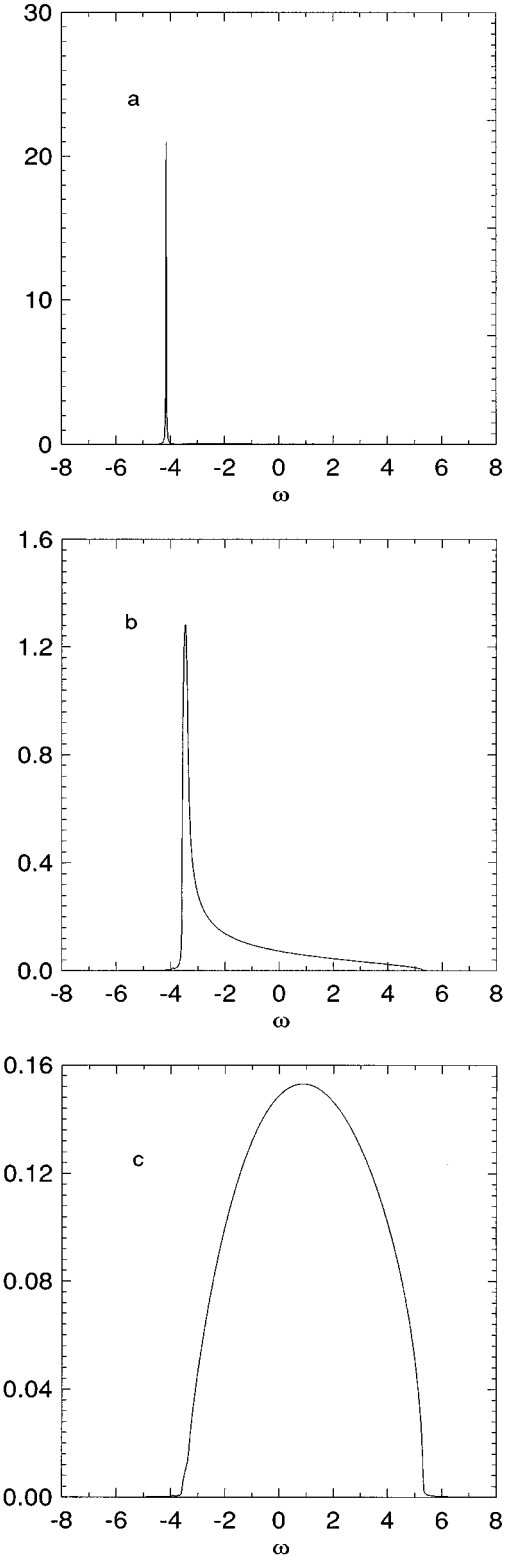

FIG. 5. The spectral functions of (a) (0,0), (b) $(4\pi/9,0)$, and (c) $(\pi,\pi/3^{1/2})$ are presented as a function of frequency. $\ell=6$, $t=-1$, and $J=0$. $\mathbf{k}=(4\pi/9,0)$ is located near the point (2,0) of Fig. 3. The quasiparticle broadens.

This fit contains hopping processes to nearest neighbors through the B term and second nearest neighbors through the C term. $B\gamma_{\mathbf{k}}$ comes from the coherent part of the Hamiltonian, whereas $Ch_{\mathbf{k}}^2$ originates from the incoherent part with the participation of quantum spin fluctuation. So at finite small J a Fermi liquid picture is appropriate to describe the motion of the hole as a quasiparticle with the dispersion relation given by (24).

For $J\gg|t|$, one gets an analytical expression for $E(\mathbf{k})$, namely,

TABLE I. The values of the coefficients α and β of Eq. (23) are reported.

k	β	α
(0,0)	0.112	1.056
$(4\pi/3,0)$	0.440	1.473
$(\pi,\pi/\sqrt{3})$	0.517	0.610

$$E(\mathbf{k}) \simeq -t\gamma_{\mathbf{k}} - \sum_{\mathbf{q}} \frac{|M(\mathbf{k},\mathbf{q})|^2}{\omega(\mathbf{q}) - t\gamma_{\mathbf{k}+\mathbf{q}}}. \tag{25}$$

C. The case of $t>0$

At finite J and positive t, the physics is similar to that of the case of $t<0$. But for $J=0$ the situation is quite different since the Nagaoka theorem is not satisfied and the energy of the hole can be minimized further in a singlet spin state. It is then natural to consider the AF background as a good approximation for $t>0$ even when $J=0$. From the calculation of the spectral function $\mathcal{A}(\mathbf{k})$, we found that the energy minimum is located at $\mathbf{k}=(0,0)$. For $\mathbf{k}=(0,0)$ $(J=0)$, a well defined quasiparticle peak is present. However, the quasiparticle is strongly **k** dependent. The peak loses in intensity and broadens, as illustrated in Fig. 5, when we move away from the center of the Brillouin zone. Therefore, depending on the wave vector, a Fermi liquid interpretation is either possible or not. We believe that Trugman processes will not spoil this conclusion since they only renormalize (slightly) the coherent part of the hole motion. This discussion raises the question of an electronic system where the quasiparticle weight depends on the wave vector **k** and vanishes on some points of the Brillouin zone.[10] Work concerning this question is in progress.

VI. EXACT DIAGONALIZATION

The exact diagonalization is performed using the Lanczos method on a 3×2^2 hexagonal cluster (Fig. 3). The dispersion relation and the total spin are calculated.

The results for $t<0$ and $t>0$ are presented. For $t<0$ the dispersion relation $E(\mathbf{k})$ and the total spin S_{tot} are summarized in Tables III and IV, respectively. $E(\mathbf{k})$ is reported as a function of the wave vector **k** and $J/|t|$. First let us consider the case $t<0$. For $0\leqslant J\leqslant 0.3$ the energies have a small dependence on **k**. But for $J>0.3$, the energy minimum is located at $\mathbf{k}=(2\pi/3,0)$ which transforms into the middle of the Brillouin zone sides, namely, $\mathbf{k}\equiv(\pi,\pi/\sqrt{3})$, by a translation $\mathbf{G}=(4\pi/3,0)$. This is consistent with what is obtained in the approach of the previous sections. However, a translation of $-\mathbf{G}$ produces a meaningless result. The reason for this discrepancy is due to the fact that in the slave fermion approach the chiral symmetry is broken, whereas in the exact diagonalization the symmetry cannot be spontaneously broken.

TABLE II. The values of the coefficients A, B, and C of Eq. (24) are reported.

J	A	B	C
0.05	-4.186	0.019	0.013
0.1	-4.018	0.032	0.025
0.2	-3.766	0.049	0.040
0.3	-3.585	0.070	0.058
0.5	-3.271	0.107	0.077

TABLE III. The hole energy as a function of **k** and J for negative t $(=-1)$ is reported.

J **k**	(0,0)	$(\pi,\pi/\sqrt{3})$	$(2\pi/3,0)$	$(4\pi/3,0)$
0.00	-6.000	-5.410	-5.662	-5.348
0.05	-5.258	-4.856	-5.040	-4.807
0.10	-4.517	-4.302	-4.418	-4.276
0.20	-3.368	-3.342	-3.349	-3.382
0.30	-2.917	-2.907	-2.898	-2.838
0.50	-2.368	-2.195	-2.454	-2.065
0.70	-1.832	-1.562	-2.073	-1.609
0.80	-1.567	-1.359	-1.895	-1.483

Things become more understandable if we calculate the total spin S_{tot}. What is clear from Table IV is that for $J>0.3$ S_{tot} is small for all the values of **k** and the ground state is a singlet: $S_{\text{tot}}=1/2$. For $0\leqslant J\leqslant 0.3$, S_{tot} is big: $5/2\leqslant S_{\text{tot}}\leqslant 11/2$. For $J=0$, the ground state, given at $\mathbf{k}=(0,0)$, is ordered ferromagnetically, a result which agrees with the Nagaoka theorem which applies only to negative t on the triangular lattice. For $0\leqslant J\leqslant 0.3$ and $\mathbf{k}\neq(0,0)$, the energies are very close to -6 (the lowest energy). The ferromagnetic states have, however, the energies 2, -1, and 3 (in units of $|t|$) for $(\pi,\pi/\sqrt{3})$, $(2\pi/3,0)$, and $(4\pi/3,0)$, respectively. A possible explanation is that the system finds a compromise in which the spins deviate slightly from the ferromagnetic state (the spins do not remain in coplanar positions) to keep a high value of S_{tot} but the energies are close to -6. This phenomenon is similar to the Aharonov-Bohm effect.[11] The stability of this phase as the size of the cluster increases has to be clarified. On the other hand, it is natural to think that the AF correlations, growing with the cluster size, will rise above any other correlations at $J>0$.

For large J, the antiferromagnetic correlations become dominant and the total spin becomes small. In this case the exact results of the minimum of the dispersion relation compare well with the self-consistent approach.

The situation is simpler for positive t. The results are summarized in Tables V and VI. There is no crossing in the energy levels as is the case for $t<0$ (Table III). The mini-

TABLE IV. The total spin as a function of **k** and J for negative t $(=-1)$ is reported.

J **k**	(0,0)	$(\pi,\pi/\sqrt{3})$	$(2\pi/3,0)$	$(4\pi/3,0)$
0.00	11/2	9/2	9/2	7/2
0.05	11/2	9/2	9/2	7/2
0.10	11/2	9/2	9/2	7/2
0.20	7/2	5/2	5/2	5/2
0.30	1/2	3/2	1/2	3/2
0.50	1/2	3/2	1/2	3/2

TABLE V. The hole energy as a function of $\mathbf{k}$ and J for positive t $(=+1)$ is reported.

J $\mathbf{k}$	(0,0)	$(\pi,\pi/\sqrt{3})$	$(2\pi/3,0)$	$(4\pi/3,0)$
0.00	-4.230	-4.120	-4.149	-4.270
0.05	-4.076	-3.928	-3.971	-4.192
0.10	-3.941	-3.760	-3.810	-4.117
0.50	-2.964	-2.706	-2.699	-3.569
2.00	0.574	0.208	0.328	-1.725
15.0	18.068	16.615	16.383	13.496

mum is always located at $\mathbf{k}=(4\pi/3,0)$ which transforms into $\mathbf{k}=(0,0)$ using Eq. (17). The total spin of the ground state is $S_{\text{tot}}=1/2$. Here also a good agreement concerning the minima of $E(\mathbf{k})$ between the two approaches is obtained. For $J=0$, the fact that the ground state is not ferromagnetic confirms that the Nagaoka theorem does not apply for $t>0$.

VII. MOTION OF A FINITE DENSITY OF HOLES

We assume that the holes exist around the minima calculated in the case of one hole. They form small pockets or valleys, whose area is proportional to their density. We shall use the slave fermion picture from now on. There is only one valley around the center of the Brillouin zone for $t>0$ but three of them on the edges of the Brillouin zone for $t<0$. We are interested in the long range interaction between holes, as mediated by low energy spin waves.

The expression of the coupling of holes to the spin waves is

$$-it\frac{\sqrt{3}}{N}\sum_{\mathbf{k},\mathbf{q}}\psi^{\dagger}_{\mathbf{k}+\mathbf{q}}\psi_{\mathbf{k}}[(u_{\mathbf{q}}h_{\mathbf{k}}-v_{\mathbf{q}}h_{\mathbf{k}+\mathbf{q}})\alpha_{\mathbf{q}} +(v_{\mathbf{q}}h_{\mathbf{k}}-u_{\mathbf{q}}h_{\mathbf{k}+\mathbf{q}})\alpha^{\dagger}_{-\mathbf{q}}]. \tag{26}$$

Among the three Goldstone modes [$\mathbf{q}=\mathbf{0}$ and $\mathbf{q}=\pm(4\pi/3,0)$], only $\mathbf{q}=\mathbf{0}$ is relevant since it is easily seen that two valleys cannot be coupled by a momentum transfer $\mathbf{q}=\pm(4\pi/3,0)$, Fig. 6, in the case $t<0$. This is *a fortiori* true in the case $t>0$ where there is only one valley left. For $\mathbf{q}\sim\mathbf{0}$, (26) becomes

$$-it\frac{\sqrt{3}}{2N}\sum_{\mathbf{k},\mathbf{q}}\psi^{\dagger}_{\mathbf{k}+\mathbf{q}}\psi_{\mathbf{k}}[h_k(u_q-v_q)(\alpha_q-\alpha^{\dagger}_{-q})]$$

$$-it\frac{\sqrt{3}}{4N}\sum_{\mathbf{k},\mathbf{q}}\psi^{\dagger}_{\mathbf{k}+\mathbf{q}}\psi_{\mathbf{k}}[(u_q+v_q)(-\mathbf{q}\cdot\boldsymbol{\nabla}h_k)(\alpha_q+\alpha^{\dagger}_{-q})] \tag{27}$$

TABLE VI. The total spin as a function of $\mathbf{k}$ and J for positive $t(=+1)$ is reported.

J $\mathbf{k}$	(0,0)	$(\pi,\pi/\sqrt{3})$	$(2\pi/3,0)$	$(4\pi/3,0)$
0.0	3/2	1/2	3/2	1/2
0.10	3/2	1/2	1/2	1/2

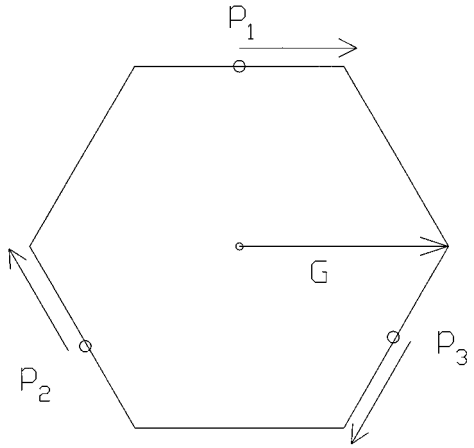

FIG. 6. The positions of the valleys and their dipolar momenta p_i are presented on the Brillouin zone for $i=1$, $i=2$, and $i=3$.

which transforms into

$$-it\frac{\sqrt{3}}{2N}\sum_{\mathbf{k},\mathbf{q}}\psi^{\dagger}_{\mathbf{k}+\mathbf{q}}\psi_{\mathbf{k}}h_k[-iS^z(q)] +t\frac{\sqrt{3}}{2N}\sum_{\mathbf{k},\mathbf{q}}\psi^{\dagger}_{\mathbf{k}+\mathbf{q}}\psi_{\mathbf{k}}\{\mathbf{p}_k\cdot[i\mathbf{q}\phi(\mathbf{q})]\} \tag{28}$$

where

$$S^z(\mathbf{q})=i(b_q-b^{\dagger}_{-q})/2 \tag{29}$$

is the slowly varying component of the magnetization in the z direction, while

$$\phi(\mathbf{q})=(b_q+b^{\dagger}_{-q})/2 \tag{30}$$

parametrizes the slow distortion of the ordered 120° sructure within its plane. The vectorial quantity

$$\mathbf{p}_k=\nabla_k h_k \tag{31}$$

appears like the effective dipolar momentum carried by the hole. It can be shown that the coupling to $S^z(\mathbf{q})$, which semiclassically behaves as $\partial\phi/\partial t$, does not lead to long range interaction between holes. On the other hand, the second term, once written in real space, becomes

$$t\frac{\sqrt{3}}{2N}\sum_{\mathbf{r}}\sum_{i}\psi_i(\mathbf{r})^{\dagger}\psi_i(\mathbf{r})[\mathbf{p}_i\cdot\boldsymbol{\nabla}_{\mathbf{r}}\phi(\mathbf{r})] \tag{32}$$

where the i indicates the different valleys (see Fig. 6). The effective dipolar momentum can safely be taken equal to its value at the center of each valley for small hole density. Two cases are to be considered.

(i) $t>0$: the minimum of the dispersion relation is located at $\mathbf{k}=\mathbf{0}$. There is only one valley and the dipolar momentum $\mathbf{p}=\mathbf{0}$. So no dipolar interaction between the holes and the spin waves can be generated. The interaction is at least quadrupolar and decays as r^{-4}.

(ii) $t<0$: the minima of the dispersion relation are located at $\mathbf{k}=(\pi,\pi/\sqrt{3})$ and equivalent momenta, Fig. 6. The dipolar momenta in this case do not vanish. They take the following values:

$$\mathbf{p}_1=2\mathbf{x},\mathbf{p}_2=-\mathbf{x}+\sqrt{3}\mathbf{y},\mathbf{p}_3=-\mathbf{x}-\sqrt{3}\mathbf{y}. \tag{33}$$

VIII. SPIRAL PHASES

According to the results of the previous sections and following the idea of Shraiman and Siggia,[3] we introduce a phenomenological Hamiltonian for the motion of a finite density of holes. The spatial density of this Hamiltonian is given by

$$\mathscr{H}=\sum_{i=1,2,3}\left\{-\frac{1}{2}\psi_i^\dagger\boldsymbol{\nabla}^2\psi_i+ga\psi_i^\dagger\psi_i(\mathbf{p}\boldsymbol{\nabla})\phi\right\}+\frac{1}{2}\left(\rho(\boldsymbol{\nabla}\phi)^2+\frac{M^2}{\chi}\right) \tag{34}$$

where M is the z component of the magnetization ($M\sim 0$). The coupling constant g is of the order of t for $t\ll J$ ($g=ta\sqrt{3}/4$). When $J\ll t$, the vertex corrections become important and are expected to renormalize g to an order of J. Using the expressions for $\mathbf{p}_1$, $\mathbf{p}_2$, and $\mathbf{p}_3$ given above, it can be seen that $\partial_x\phi$ and $\partial_y\phi$ are respectively coupled to $2n_1-n_2-n_3$ and $\sqrt{3}(n_2-n_3)$ where $n_i=\langle\psi_i^\dagger\psi_i\rangle$ is the hole density in the valley i. At the mean-field level, we can write

$$\mathscr{H}_{\rm int}=ga\,\mathrm{Re}\{(n_1+n_2e^{-2i\pi/3}+n_3e^{2i\pi/3})(\partial_x\phi+i\partial_y\phi)\}+|\partial_x\phi+i\partial_y\phi|^2. \tag{35}$$

The minimization with respect to ϕ yields

$$\partial_x\phi+i\partial_y\phi=-\frac{ga}{\rho}(n_1+n_2e^{-2i\pi/3}+n_3e^{2i\pi/3}). \tag{36}$$

Equation (35) becomes

$$\mathscr{H}_{\rm int}=-\frac{1}{2}\frac{g^2a^2}{\rho}|n_1+n_2e^{-2i\pi/3}+n_3e^{2i\pi/3}|^2 \tag{37}$$

and the kinetic energy can be written as follows:

$$\frac{\pi}{m}(n_1^2+n_2^2+n_3^2)=\frac{\pi}{3m}[(n_1+n_2+n_3)^2+2|n_1+n_2e^{-2i\pi/3}+n_3e^{2i\pi/3}|^2] \tag{38}$$

so that the normal phase becomes unstable when

$$\frac{2\pi}{3m}-\frac{1}{2}\frac{g^2a^2}{\rho}<0,$$

that is, when $3g^2a^2m/\rho\pi$. Once this condition is satisfied, the system maximizes

$$|n_1+n_2e^{-2i\pi/3}+n_3e^{2i\pi/3}|^2=\frac{1}{2}[(n_1-n_2)^2+(n_2-n_3)^2+(n_3-n_1)^2].$$

This is realized for $n_1=n>0$ and $n_2=n_3=0$ or all the solution obtained by cyclic permutation of the indices 1, 2, and 3. This implies that only one valley is occupied and the two others are empty in the spiral phase. A simple interpretation of this phase in the real space is obtained using Eq. (36). For the phase $n_1=n$ and $n_2=n_3=0$ one has

$$\langle\partial_x\phi\rangle=-\frac{ga}{\rho}n \text{ and } \langle\partial_y\phi\rangle=0,$$

which means that the spins rotate around their position in the normal phase uniformly when moving along the x axis. In the other solutions for n_i, the rotation occurs along the axes $\mathbf{e}_2$ and $\mathbf{e}_3$ for $n_1=n_3=0$ and $n_2=n$, and $n_1=n_2=0$ and $n_3=n$, respectively.

ACKNOWLEDGMENTS

We are grateful to J. C. Angles D'Auriac for helpful and interesting discussions. One of us (M.A.) would like to thank the Natural Sciences and Engineering Research Council of Canada (NSERC) and the Fonds pour la formation de chercheurs et l'aide a la recherche from the Government of Québec (FCAR) for financial support.

[1] P. W. Anderson, Science **235**, 1196 (1987).
[2] D. A. Huse and V. Elser, Phys. Rev. Lett. **60**, 2531 (1988); S. Tang and J. E. Hirsh, Phys. Rev. B **39**, 4548 (1989); B. Bernu, C. L'Huillier, and L. Pierre, Phys. Rev. Lett. **69**, 2590 (1992).
[3] B. I. Shraiman and E. D. Siggia, Phys. Rev. Lett. **62**, 1564 (1989).
[4] D. P. Arovas and A. Auerbach, Phys. Rev. B **38**, 316 (1988).
[5] W. F. Brinkman and T. M. Rice, Phys. Rev. B **2**, 1324 (1970).
[6] G. Martinez and P. Horcsh, Phys. Rev. B **44**, 317 (1991).
[7] S. A. Trugman, Phys. Rev. B **37**, 1597 (1988).
[8] H. Tasaki, Phys. Rev. B **40**, 9192 (1989).
[9] M. Azzouz, Ph.D. thesis, Université Joseph Fourier, Grenoble, 1992.
[10] M. Azzouz (unpublished).
[11] B. Doucot and R. Rammal, Phys. Rev. B **41**, 9617 (1990).